Article

Individualized low-dimensional carbon allotropes: Enabling ground state and excited state charge transfer by molecular heptamethine cyanine

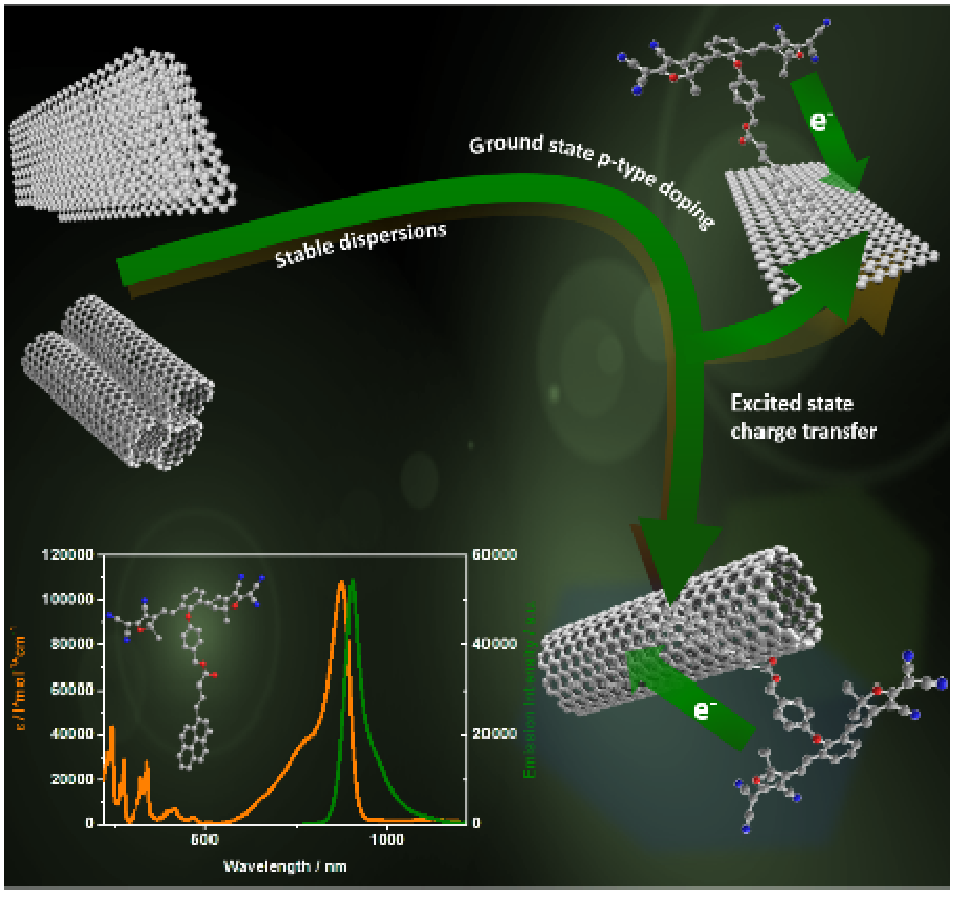

Alexandra Roth, Christoph Schierl, Andrés Ferrer-Ruiz, Martin Minameyer, Laura Rodríguez-Pérez, Carmen Villegas, Mª Ángeles Herranz, Nazario Martín and Dirk M. Guldi

maherran@ucm.es (M. A. H.)
nazmar@ucm.es (N. M.)
dirk.guldi@fau.de (D. M. G.)

HIGHLIGHTS

Heptamethine cyanine dyes endowed with pyrene anchoring groups form stable supramolecular aggregates with SWCNTs and NG

The electron donating character of heptamethine cyanines enables the *n*-doping of carbon allotropes

Statistical Raman analysis is a powerful technique to investigate doping effects in carbon nanomaterials

Transient absorption spectroscopy allows the investigation of the shift/transfer of charge in the ground/excited tates

Single walled carbon nanotubes (SWCNTs) and nanographene (NG) interact supramolecularly, via π–π stacking forces, with an anionic heptamethine cyanine NIR-dye forming stable assemblies. The electron donating character of the dye, especially when combined with both SWCNTs and NG, was corroborated by Raman and transient absorption spectroscopies. Result from the electronic interaction is the observed shift of charge density from the dye to SWCNTs in the electronically dark state and a noticeable charge transfer upon photoexcitation.

Article

Individualized low-dimensional carbon allotropes: Enabling ground state and excited state charge transfer by molecular heptamethine cyanine

Alexandra Roth,[1,4] Christoph Schierl,[1,4] Andrés Ferrer-Ruiz,[2,4] Martin Minameyer,[1] Laura Rodríguez-Pérez,[2] Carmen Villegas,[2] Mª Ángeles Herranz,[2,*] Nazario Martín[2,3,5,**] and Dirk M. Guldi[1,*]

[1]Department of Chemistry and Pharmacy and Interdisciplinary Center for Molecular Materials, University of Erlangen-Nuremberg Egerlandstrasse 3, 91058 Erlangen (Germany).
[2]Departamento de Química Orgánica I, Facultad de Química Universidad Complutense, 28040 Madrid, Spain
[3]IMDEA-Nanociencia, c/Faraday 9, Campus Cantoblanco, 28049 Madrid, Spain
[4]Co-first authors
[5]Lead Contact
*Correspondence: maherran@ucm.es,dirk.guldi@fau.de
**Correspondence: nazmar@ucm.es

SUMMARY

Individualized single walled carbon nanotubes (SWCNTs) and exfoliated nanographene (NG) have been probed in the context of supramolecular interactions with an anionic heptamethine cyanine NIR-dye. The outstanding light-harvesting capability of the heptamethine cyanine permits to easily monitor the formation of the supramolecular hybrids by UV-Vis-NIR. Raman spectroscopy studies evidenced upshifted 2D bands and downshifted G bands for the obtained hybrids, which indicate the electronic n-doping of the carbon nanostructures caused by the heptamethine cyanine assembly. Furthermore, the electron donating character of the heptamethine cyanine in combination with SWCNTs and NG was corroborated in terms of a shift of charge density in the dark and in a transfer of charges upon photoexcitation.

KEYWORDS

Carbon nanotubes, graphene, light harvester, cyanines, supramolecular chemistry, organic electronics, Raman spectroscopy, n-doping, transient absorption spectroscopy, electron transfer.

INTRODUCTION

Low-dimensional carbon allotropes including fullerenes,[1] single walled carbon nanotubes (SWCNT),[2,3,4] and nanographene (NG),[5] represent interesting nanoscale building blocks, since they feature physical and chemical properties, which are of tremendous interest for applications in the emerging field of nanotechnology.[6,7,8] The most prominent examples for applications are found in the areas of organic solar cells,[9,10] ultrasensitive biosensors,[11,12,13] fuel cells,[14,15,16] conductive electrodes for touch screens,[17] and field-effect transistors devices[18] To this date, exploring the full potential of SWCNTs and graphene constitutes one of the biggest challenges in the field. A clear bottleneck is their individualization/exfoliation in combination with their stabilization in dispersion.

In recent years, the chemical functionalization, that is, covalent and noncovalent chemistry of SWCNTs and NG, has led to remarkable advances in the field.[19] For instance, covalent functionalization of SWCNTs or NG with functional entities enables solubilizing/dispersing them in common solvents.[20,21] The side effects of most chemical functionalization reactions are the uncontrolled modification of the extended carbon network, in general, and the π-conjugation, in particular. Notable is also the arbitrary alteration of the electronic structure, which is shown in the case of SWCNTs to lead to a complete loss of absorption and fluorescence. On the contrary, noncovalent functionalization enables the immobilization of functional entities via π-π stacking, hydrophobic, and charge transfer interactions or any combination of the aforementioned, without, however, any of these unwanted side effects.[22,23,24,25] In this context, the role of planar and aromatic building blocks such as porphyrins,[26] pyrene derivatives,[23,27,28,29] perylene diimides,[30] and conjugated polymers,[31,32] which all exhibit

The Bigger Picture

To control the electronic properties of carbon nanostructures, doping is one of the most feasible methods. In particular, the chemical modification by non-covalent approaches allows to fine-tune the type and the concentration of carriers without affecting the conjugated carbon sp^2 frameworks.
Functionalization schemes that besides the doping effect confer an additional element of control over the nanomaterial properties are particularly attractive and, in this sense, the combination of carbon nanostructures with photo- and electroactive molecules attracts considerable attention for their potential for artificial photosynthesis or in photovoltaics.
Such design principles have been considered for the construction of the nanomaterials here presented, where single walled carbon nanotubes (SWCNTs) and nanographene (NG) form stable supramolecular hybrids with heptamethine cyanine NIR-dyes. We have studied the excited-state dynamics and established the presence of charge transfer processes that can set the foundation for developing nanomaterials to be incorporated in next-generation devices.

strong affinities to interact with SWCNTs and NG, has been particularly beneficial in terms of stability. Noncovalent functionalization assists in blending the intrinsic properties of SWCNTs or NG with those of virtually any other functional entity. Solubility/dispersability, next to electron donation/electron withdrawal or light harvesting, stands out among the properties.[33,34]

In recent years, the chemical functionalization, that is, covalent and noncovalent chemistry of SWCNTs and NG, has led to remarkable advances in the field.[19] For instance, covalent functionalization of SWCNTs or NG with functional entities enables solubilizing/dispersing them in common solvents.[20,21] The side effects of most chemical functionalization reactions are the uncontrolled modification of the extended carbon network, in general, and the π-conjugation, in particular. Notable is also the arbitrary alteration of the electronic structure, which is shown in the case of SWCNTs to lead to a complete loss of absorption and fluorescence. On the contrary, noncovalent functionalization enables the immobilization of functional entities via π-π stacking, hydrophobic, and charge transfer interactions or any combination of the aforementioned, without, however, any of these unwanted side effects.[22,23,24,25] In this context, the role of planar and aromatic building blocks such as porphyrins,[26] pyrene derivatives,[23,27,28,29] perylene diimides,[30] and conjugated polymers,[31,32] which all exhibit strong affinities to interact with SWCNTs and NG, has been particularly beneficial in terms of stability. Noncovalent functionalization assists in blending the intrinsic properties of SWCNTs or NG with those of virtually any other functional entity. Solubility/dispersability, next to electron donation/electron withdrawal or light harvesting, stands out among the properties.[33,34]

In the current work, we have explored the synthesis of a novel cyanine-pyrene conjugate and, subsequently, the interactions with low-dimensional carbon allotropes. This is meant to realize stable electron-donor acceptor hybrids in dispersions. On one hand, pyrene as a π-π stacking anchor is known for its strong affinity to π-conjugated carbon networks.[35,36,37] On the other hand, cyanines are a class of ionic light harvester with a carbon skeleton of an odd number of π-conjugated carbon atoms. They exhibit unique absorption properties with high extinction coefficients in the near infrared region and good chemical stability. The absorption maxima of heptamethine cyanines are located at wavelengths of 750 nm and beyond, while their extinction coefficients exceed 105 $M^{-1}cm^{-1}$. By virtue of their electron donating strength they have emerged as a complement to fullerenes, which are the omnipresent electron acceptors in solar energy conversion schemes.[38,39] Importantly, electronic interactions between SWCNTs/NG and heptamethine cyanine are traceable by Raman spectroscopy, which, in the current work, allows to corroborate the n-doping of the carbon allotropes. In the case of SWCNTs, which are intrinsically p-doped, molecular n-doping is rather scarce.

RESULTS AND DISCUSSION

The synthesis of the electron donating cyanine-pyrene **1** was based on an esterification reaction between a previously synthesized 4-hydroxybenzyl-cyanine[40] and 1-pyrene butyric acid in the presence of N-[3-(diethylamino)propyl]-N'-ethylcarbodiimide hydrochloride (EDC·HCl) and 4-dimethylaminopyridine (DMAP) with a 66% yield (Scheme 1). The structure of **1** was confirmed by standard spectroscopic techniques including FTIR, ^{1}H NMR, ^{13}C NMR, UV–Vis-NIR, and high-resolution MS – see Experimental Procedures for details.

From steady state absorption, spectroscopy, maxima for **1** in methanol are observed between 230-350 nm which relate to the pyrene anchor. A strong absorption at 874 nm is, however, associated with the heptamethine cyanine. Moreover, also fluorescence measurements of **1** were conducted. Figure S1 (Supplemental Information) documents that regardless of exciting pyrene or heptamethine cyanine, a strong near-infrared fluorescence of the latter evolves. As such, an energy transfer from pyrene activates the heptamethine cyanine centered fluorescence. In line with an energy transfer are fluorescence quantum yields of 0.05% and 4.5% for the pyrene and heptamethine cyanine fluorescence, respectively. Turning to electrochemistry, **1** was investigated in a oDCB/acetonitrile solvent mixture 4/1 (v/v). Reductions were observed at -1.19 and -2.00 V, while three oxidations are seen at -0.06, +0.49, and +0.77 V – all versus Fc/Fc^{+}. With regard to the electron donor strength, we turned to spectroelectrochemical oxidation of **1** in methanol with $TBAPF_6$ as supporting electrolyte. The differential absorption spectra – Figure S2 (Supplemental Information) – were obtained by applying a potential of 0.45 V versus an Ag-wire. An intense bleaching of the ground state absorption at 874 nm of 1 is discernable. In addition, new absorption maxima emerge at 513, 540, 585, 641 nm, and at 1068 nm. Finally, femtosecond transient absorption spectroscopic measurements were conducted. The differential absorption spectra of **1** in methanol, which

are shown in Figure S3 (Supplemental Information), reflect the absorption characteristics of the singlet excited state as they develop immediately after 387 nm excitation. New maxima at 554, 614, and 1246 nm, new shoulders at 494, 561, and 625 nm, and a new minimum at 893 nm are discernable. Please note that the 893 nm minimum is accompanied by a 972 nm shoulder as a superimposition of ground state bleaching and stimulated fluorescence. Information regarding the deactivation was derived from global fitting. As a matter of fact, a short-lived and a long-lived component of 3.4 and 171 ps, respectively, were obtained (Figure S4, Supplemental Information). The short-lived component is due to the population of the first singlet excited state, which is most likely formed by vibrational relaxation. Following its formation, the first singlet excited state decays via recovery of the ground state. This is the long-lived component.

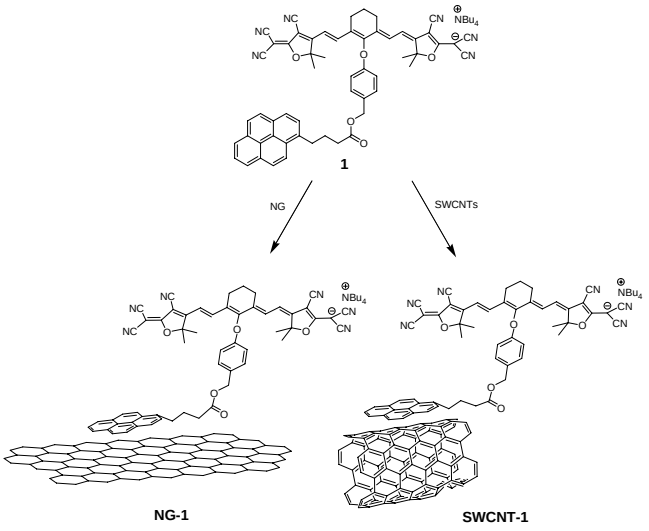

Scheme 1. Supramolecular functionalization of SWCNTs and NG with heptamethine cyanines
Schematic representation of π-π stacking interactions of **1** with SWCNTs and NG to afford **SWCNT-1** and **NG-1**, respectively.

Next, protocols for forming hybrids of **1**, with either SWCNTs (**SWCNT-1**) or NG (**NG-1**), were developed[41] – see Experimental Procedures for details. The stepwise hybrid formation was monitored by steady state absorption as well as by fluorescence spectroscopy. Figure 1 documents that the original absorption features of **1** at 874 nm decreased upon addition of SWCNTs/NG, while a new absorption feature grows at 944 nm. Moreover, the fluorescence of **1** is completely quenched upon the final enrichment step (Figure S5, Supplemental Information). The impact of the hybrid formation on the SWCNTs centered transitions were investigated in titration assays. By means of stepwise addition of **1** to predispersed SWCNTs in methanol any influence stemming from an improved debundling of SWCNTs could be excluded. As such, the red shifts of, for instance, the (7,6)-SWCNTs centered transition from 1169 nm to 1175 nm (Figure S6, Supplemental Information) during the course of titration corroborates mutual interactions between **1** and SWCNTs.

To rule out possible decompositions of **1** during **SWCNT-1** or **NG-1** formation, they were disintegrated into the individual components. We opted for Tween 60 – a non-ionic surfactant – to convert **SWCNT-1** and **NG-1** to SWCNTs, NG, and **1** – Figures S7 and S8 (Supplemental Information) – and to monitor the absorption spectra. Thereby, the recovery of the initial absorption spectrum of **1** upon Tween 60 addition corroborates the fact that **SWCNT-1** and **NG-1** are based on noncovalent forces between **1** and SWCNTs/NG. Furthermore, the formation of the hybrid systems was corroborated by thermogravimetric analysis (TGA) under inert conditions. The decomposition of **1** occurs in two steps, namely at 195.5 ºC and 289.4 ºC, leading to an overall weight loss of 85%. In contrast, SWCNTs and NG are stable up to 800 ºC with minor weight losses of 6.82% and 11.73%, respectively (Figures S9 and S10, Supplemental Information). For **SWCNT-1** and **NG-1** an additional weight loss is observed, this is likely to correspond to the release of **1** from the surface of SWCNTs (Figure S9, Supplemental Information) or NG (Figure S10, Supplemental Information). The desorption of **1** in **SWCNT-1** causes a weight loss of 11.52%, which translates to a ratio of a single molecule of **1** per 750 carbon atoms of SWCNTs and likewise, for **NG-1** an additional 14.05% weight loss relative to that of NG can be related to one molecule of 1 per 578 carbon atoms. FTIR and XPS provided further compositional

information regarding **SWCNT-1** and **NG-1**. In the FTIR of the two hybrids, carbonyl and cyano functional groups can be easily identified by their stretching bands at 1736 cm^{-1} and 2214 cm^{-1}, respectively (Figure S11, Supplemental Information). Furthermore, evidence of the carbon nanomaterial presence is gathered. In this regard, the in-plane vibration band of C=C is recognized at 1575 cm^{-1} for **SWCNT-1** and at 1584 cm^{-1} for **NG-1**. The aliphatic C-H stretching bands, at ca. 2850–2950 cm^{-1}, and the bending bands at ca. 1250–1500 cm^{-1}, were also discernible.

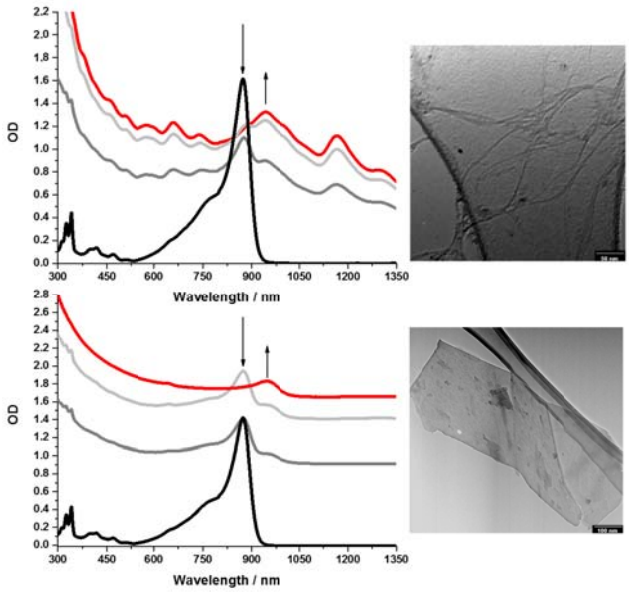

Figure 1. Absorption spectra (left) and TEM images (right) of SWCNT-1, NG-1 and reference materials
Absorption spectra of **1** (black) and **SWCNT-1** (upper)/**NG-1** (lower) (grey, light grey and red) for 3 enrichment cycles in methanol. TEM images of **SWCNT-1** (upper, scale bar 50 nm) and of **NG-1** (lower, scale bar 100 nm).

XPS elemental compositions of **1**, **SWCNT-1** and **NG-1** are based on the element signals for C (1s), N (1s) and O (1s) at 284.6, 398.6 and 532.6 eV, respectively (Figure S12, Supplemental Information). The high-resolution C 1s core-level spectra of **SWCNT-1**/**NG-1** are interpreted in terms of photoelectrons originating from sp^2 carbon atoms, sp^3 carbon atoms, and oxidized carbon atoms as part of C–O/C-N and C=O bonds. In the O 1s spectra, signals at 531.4 and 532.1 eV are assigned to C=O surface groups and C-O groups, respectively. Finally, the high-resolution N 1s core-level spectra analysis shed light onto three different contributions: 403.1, 399.7, and 398.8 eV for **NG-1** and **SWCNT-1** (Figure S12, Supplemental Information). The first is attributed to quaternary ammonium salts. The second is assigned to cyano groups as integrative parts of the cyanine core and the third is assigned to cyano groups, which are shifted towards lower binding energies because they are predominantly involved in the stabilization of the negative charge density of the cyanine.[42,43]

Microscopic insights into **SWCNT-1** as well as **NG-1** prepared in methanol solutions and drop casted onto lacey carbon coated copper grids were obtained by TEM – Figure 1. The enhanced stability of **SWCNT-1** and **NG-1** dispersions is confirmed when comparing them with SWCNTs and NG dispersions, which reveal aggregation on a time scale of a few minutes (Figure S13, Supplemental Information). For **SWCNT-1**, TEM images point to debundling of SWCNTs and to the coexistence of individual **SWCNT-1** and smaller bundles of SWCNTs/**SWCNT-1**. When turning our attention to **NG-1**, exfoliation of graphite is documented by the existence of barely restacked, turbostratic NG due to interactions with **1**. For the references, a poor stabilization of individualized SWCNTs and exfoliated NG by means of the solvent is observed in the form of rebundling or restacking, (Figures S14 and S15, Supplemental Information). Insights into doping effects are gathered from statistical analysis of the measured Raman data. Due to an altered sample preparation, no single layer graphene or highly debundled SWCNTs are expected to be found in these measurements – for preparation details see Experimental Procedures. These analyses were conducted by measuring about 1000 spectra of each sample with 532 nm or 633 nm laser excitation. Cluster analyses of SWCNTs and NG reference systems as well as **SWCNT-1** and **NG-1** were applied and compared. In Figure 2, the resulting mean spectra for SWCNTs and **SWCNT-1** as well as NG and **NG-1** are illustrated. In terms of SWCNTs and **SWCNT-1**, the radial breathing modes (RBM) for (8,7) and (7,6) SWCNTs were detected at 222 and 258.5 cm^{-1} for

SWCNTs and at 220 and 258 cm^{-1} for **SWCNT-1**. A comparison of the G- and 2D-modes at 1591 and 2607 cm^{-1}, respectively, for SWCNTs indicates downshifts for **SWCNT-1**. In particular, the G-mode shifts to 1588 cm^{-1}, while the 2D-mode is seen at 2604 cm^{-1}. In sound agreement with recent reports, we ascribe the down-shifts in **SWCNT-1** relative to SWCNTs to an n-type doping.[44,45] In terms of NG and **NG-1**, the D-modes were found in both cases at 1343 cm^{-1}, whereas subtle shifts evolve for the G- and 2D-modes. The G-modes are observed at 1576 and 1572 cm^{-1} and the 2D-modes at 2680 and 2695 cm^{-1} for NG and **NG-1**, respectively. Our results, namely an upshifted 2D-mode in combination with a downshifted G-band, indicate also a n-type doping of this carbon allotrope.[46]

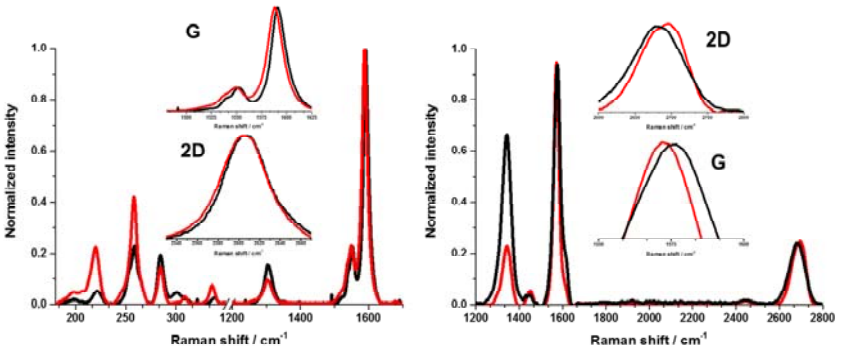

Figure 2. Raman spectra of SWCNT-1 and NG-1
Mean Raman spectra of SWCNTs (black) and **SWCNT-1** (red) following 633 nm excitation (left) and of NG (black) and **NG-1** (red) following 532 m excitation (right), which were recorded after drop casting them onto Si/SiO_2 wafer. Zoom-ins: G- and 2D-modes to illustrate the shifts.

Insights into the excited state dynamics of **SWCNT-1** and **NG-1** were gathered in transient absorption measurements, which were analysed by global and target analyses. Figure 3 shows deconvoluted transient absorption spectra of **SWCNT-1** and **NG-1** obtained by target/global analysis and their corresponding concentration-time profiles. At first glance, none of them reveal the characteristic fingerprints of photoexcited **1** – vide supra. The lack of the ground state bleaching of **1** at 874 nm, confirms the absence of any free, non-immobilized **1**. Instead, the bleaching is in line with the ground state absorptions of **SWCNT-1** and **NG-1** red-shifted to 944 and 947 nm. Figures S18 and S20 (Supplemental Information) show the corresponding evolution associated spectra following 387 nm excitation of the SWCNTs and NG references. In the case of SWCNTs, an instantaneous formation of minima at 665, 743, 1017, 1170 and 1312 nm that correspond to the ground state bleaching of the S22 and S11 transitions is discernible (Figure S16, Supplemental Information). In line with improved debundling observed in microscopy, these are hypsochromically shifted for **SWCNT-1** to 661, 738, 1006, 1156, and 1302 nm (Figure S19, Supplemental Information). Global and target analysis gave lifetimes of 0.4 / 1.89 / 115 ps for SWCNTs and 0.37 / 1.77 / 59 ps as well as 2.40 ns for **SWCNT-1**, while that of **1** are 3.4 and 175 ps. Turning to NG and **NG-1**, in both cases the broad and featureless negative transients in the near-infrared, which are caused by phonon-related bleaching of NG, are discernable (Figure S17, Supplemental Information). For this bleaching, a lifetime of 1.7 ps and of 1.4 ps has been determined in the case of NG and **NG-1**, respectively. Next to the rather broad bleaching, new distinct features in the form of a minimum at 944 nm and a maximum at 996 nm are seen for **NG-1** (Figure S21, Supplemental Information). No such transients are, however, found for **1** or NG. From global analysis we derive a lifetime of 2.63 ns for the latter transient.

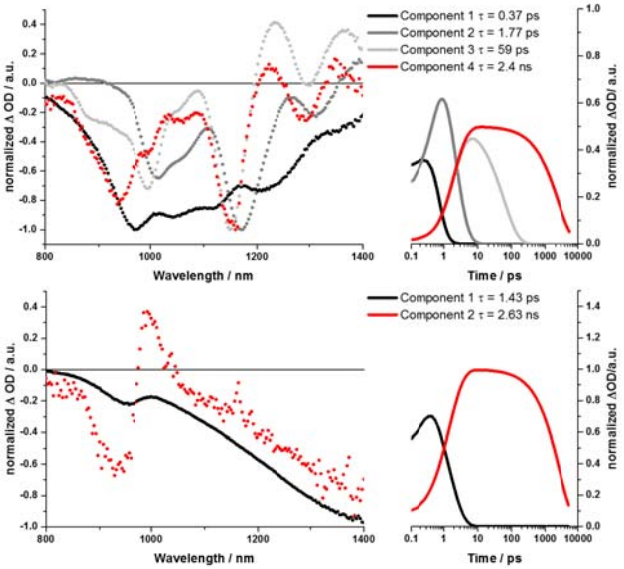

Figure 3. Deconvoluted transient absorption spectra of SWCNT-1 and NG-1
Left: Deconvoluted transient absorption spectra of **SWCNT-1** (upper) and **NG-1** (lower) obtained by target/global analysis. Right: Corresponding concentration-time profiles of **SWCNT-1** (upper) and **NG-1** (lower).

The decay and evolution associated spectra (DAS/EAS) of **SWCNT-1** and **NG-1** related to the longest lifetimes have both a minimum at 944 nm and a maximum at around 996 nm which resemble the pattern of oxidized **1**. It is slightly superimposed by SWCNTs centered transients in **SWCNT-1**. Taking the aforementioned into concert, we reach the conclusion that photoexciting **SWCNT-1** and **NG-1** is in both cases the inception to an ultrafast charge separation. As such radical ion pair state species are formed, in which **1** is oxidized and either SWCNTs or NG are reduced. Charge recombination is with 2.40 and 2.63 ns much slower and affords the ground state.

In summary, we have synthetized a novel conjugate **1** by linking pyrene as an anchor with an anionic heptamethine cyanine as an electron donor to enable π-π stacking onto low-dimensional carbon allotropes and to redistribute electron density with the latter, respectively. Complementary investigations were based on microscopic and spectroscopic assays to shed light onto individualizing SWCNTs and exfoliating graphite by means of **1**, on one hand, and n-type doping of individualized SWNCTs and exfoliated NG, on the other hand. By means of microscopic analyses the individualization of SWCNTs and exfoliation of graphite as well as the stability of the resulting dispersions was confirmed. Spectroscopic analyses corroborated in **SWCNT-1** and **NG-1** the shift of partial electron density from **1** to SWCNTs/NG in the electronically dark state and the shift of full electron density in the electronically excited state. The earlier shift with characteristics of a charge transfer state is stable, while the latter is a charge separated state and is nanoseconds lived.

EXPERIMENTAL PROCEDURES

Synthesis of 1

1-Pyrene butyric acid (0.12 mmol), *N*-[3-(diethylamino)propyl]-*N'*-ethylcarbodiimide hydrochloride (EDC·HCl) (0.12 mmol) and 4-(dimethylamino)-pyridine (DMAP) (0.12 mmol) were added to 30 mL of CH_2Cl_2. The mixture was stirred for 20 min. at 0 ºC (ice/water bath) under Ar. Afterwards, 4-hydroxybenzyl-cyanine[40] (0.09 mmol) was added dropwise and the mixture was stirred for another 30 min. The cooling bath was removed and the mixture was stirred at room temperature for 24 h. The reaction mixture was washed with deionised water (4 x 30 mL). The organic layer was dried over $MgSO_4$, filtered and evaporated. The residue was subjected to column chromatography in CH_2Cl_2/MeOH 9/1 for further purification. Yield: 66 %. ^{1}H NMR (300 MHz, DMSO-d_6): δ = 8.40–7.91 (m, 9H, Ar-CH), 7.61 (d, *J* = 14.0 Hz, 2H, CH), 7.32 (d, *J* = 8.0 Hz, 2H, Ar-CH), 6.95 (d, *J* = 7.7 Hz, 2H, Ar-CH), 5.93 (d, *J* = 14.0 Hz, 2H, CH), 5.02 (s, 2H, CH_2), 3.21–3.09 (m, 8H, CH_2), 2.56 (m, 2H, CH_2), 1.99 (m, 6H, CH_2), 1.85 (m, 2H, CH_2), 1.56 (m, 8H, CH_2), 1.31 (s, 12H, CH_3), 1.26-1.23 (m, 8H, CH_2), 1.17 (t, *J* = 7.0 Hz, 2H, CH_2), 0.94 (t, *J* = 7.0 Hz, 12H, CH_3). ^{13}C NMR (75 MHz THF-d_8,): δ = 173.41, 137.21, 132.63, 132.17, 131.46, 131.25, 131.18, 129.86, 128.50, 128.42, 128.28, 127.58, 126.78, 126.15, 126.07, 125.90, 125.80, 125.71, 124.44, 116.03, 95.22, 66.23, 59.45, 34.41, 33.59, 28.09, 27.19, 20.74, 14.14. UV-Vis

(oDCB) λ_{max}: 906 (ε= 254000 $L \cdot mol^{-1} \cdot cm^{-1}$), 346, 331 nm. FTIR (KBr): 2928, 2208, 1730, 1625, 1504, 1438, 1335,1254, 1214, 1080, 1038, 1000, 903, 840, 729, 648 cm^{-1}. HRMS. (ESI^-): m/z calculated for $C_{57}H_{43}N_6O_5^-$ = 891.3300; found = $C_{57}H_{43}N_6O_5^-$ = 891.3297.

SWCNT/NG references preparation. For the preparation of SWCNTs and NG dispersions the pristine graphite or SWCNTs were added to either methanol or anhydrous *o*DCB and dispersed by bath sonication. Following sonication, the resulting dispersions were centrifuged and the supernatant separated from the precipitate. The former was used for further characterization or hybrid formation.

SWCNT-1/NG-1 supramolecular hybrids preparation. SWCNT-1 as well as **NG-1** were produced via similar procedures. A solution of **1** was prepared and pristine SWCNTs or graphite were added. The resulting mixtures were ultrasonicated in an ultrasonication bath. Furthermore, the hybrid formation could be either done stepwise, where SWCNTs or graphite flakes were added in small portions to the solution of **1** with intermediate ultrasonication steps until no free **1** was in solution anymore, or by adding an excess of **1** to SWCNT or NG dispersions followed by only one sonication step. In the latter case, a filtration step is added in contrast to the first option, where the samples are centrifuged in the last step to remove non exfoliated graphite flakes or bundled SWCNTs.

To avoid misinterpretations due to differences in debundling or exfoliation in the case of Raman measurements, the sample preparation differs from the aforementioned cycle enrichments. Here, SWCNTs and NG were sonicated in methanol and, drop casted onto Si/SiO_2 wafers as references. Subsequently, SWCNT and NG coated wafers prepared in the same way, were treated with a concentrated methanol solution of **1**.

SWCNT-1. FTIR (KBr): ν = 2924, 2214, 1736, 1635, 1575, 1456, 1401, 1055 cm^{-1}; TGA: weight loss and temperature desorption (organic anchoring groups): 11.52 %, 650 °C; XPS: % atomic: C (284.6 eV) = 93.14, N (398.6 eV) = 1.15, O (532.6 eV) = 5.11.

NG-1. FTIR (KBr): ν = 2934, 2214, 1736, 1628, 1584, 1404, 1384, 1117, 1050, 712, 623 cm^{-1}; TGA: weight loss and temperature desorption (organic anchoring groups): 14.05 %, 650 °C; XPS: % atomic: C (284.6 eV) = 94.76, N (398.6 eV) = 1.09, O (532.6 eV) = 4.14.

SUPPLEMENTAL INFORMATION

Supplemental Information includes Materials and Methods, Instruments and twenty three figures that can be found with this article online.

AUTHOR CONTRIBUTIONS

Experiments were conceived and designed by M.A.H., N.M. and D.M.G. D.M.G. and N.M. acquire the financial support for the project. The materials were synthesized by A.R., C.S. and A.F.-R. Spectroscopy and data analysis were carried out by A.R., C.S., A.F-R., M.M., L.R.-P. and M.A.H. All authors wrote and commented on the manuscript.

ACKNOWLEDGMENTS

This work was supported by the Deutsche Forschungsgemeinschaft as part of the Excellence Cluster Engineering of Advanced Materials and SFB 953 Synthetic Carbon Allotropes as well as by the Bavarian State Government as part of the Solar Technologies go Hybrid initiative. Financial support from the European Research Council (ERC-320441-Chiralcarbon), the Ministerio de Economía y Competitividad (MINECO) of Spain (Projects CTQ2014-52045-R and CTQ2015-71936-REDT) and the CAM (PHOTOCARBON project S2013/MIT-2841) is also acknowledged. C.S. gratefully acknowledges the Fonds der Chemischen Industrie (FCI) for funding

REFERENCES AND NOTES

1. Kroto, H. W., Heath, J. R., O'Brien, S. C., Curl, R. F., and Smalley, R. E. (1985). C_{60}: buckminsterfullerene, Nature, *318*, 162-163.
2. Iijima, S. (1991). Helical microtubules of graphitic carbon. Nature , *354*, 56-58.
3. Iijima, S., and Ichihashi, T. (1993). Single-shell carbon nanotubes of 1-nm diameter. Nature, *363*, 603-605
4. Bethune, D. S., Klang, C. H., de Vries, M. S., Gorman, G., Savoy, R., Vazquez, J., and Beyers, R. (1993) Cobalt-catalysed growth of carbon nanotubes with single-atomic-layer walls. Nature. *363*, 605-607.
5. Geim, A. K., and Novoselov, K. S. (2007). The rise of graphene. Nat. Mater. *6*, 183-191.
6. Sharon, M.,and Sharon, M. (2009). Carbon Nano Forms and Applications. (McGraw-Hill Education).
7. Guldi, D. M., and Martín, N. (2010). Carbon Nanotubes and Related Structures: Synthesis, Characterization, Functionalization, and Applications. (Wiley).
8. Akasaka, T., Wudl, F., and Nagase, S. (2010). Chemistry of Nanocarbons. (Wiley).
9. Chang, D. W., Choi, H.J., Filer, A., and Baek, J.B. (2014). Graphene in photovoltaic applications: Organic photovoltaic cells (OPVs) and dye-sensitized solar cells (DSSCs). J. Mater. Chem. A. *2*, 12136-12149.

10. Martín, N. (2017). Carbon Nanoforms for Photovoltaics: Myth or Reality? Adv. En. Mater., DOI: 10.1002/aenm.201601102.
11. Zan, X., Bai, H., Wang, C., Zhao, F., and Duan, H. (2016). Graphene Paper Decorated with a 2D Array of Dendritic Platinum Nanoparticles for Ultrasensitive Electrochemical Detection of Dopamine Secreted by Live Cells. Chem. Eur. J., *22*, 5204-5210.
12. Shi, J., Li, X., Chen, Q., Gao, K., Song, H., Guo, S., Li, Q., Fang, M., Liu, W., Liu, et al. (2015). A monocrystal graphene domain biosensor array with differential output for real-time monitoring of glucose and normal saline. Nanoscale, *7*, 7867-7872.
13. Zhu, A. Y., Yi, F., Reed, J. C., Zhu, H., and Cubukcu, E. (2014). Optoelectromechanical Multimodal Biosensor with Graphene Active Region. Nano Lett. *14*, 5641-5649.
14. Yang, L., Wang, S., Peng, S., Jiang, H., Zhang, Y., Deng, W., Tan, Y., Ma, M., and Xie, Q. (2015). Facile Fabrication of Graphene-Containing Foam as a High-Performance Anode for Microbial Fuel Cells. Chem. Eur. J. *21*, 10634-10638.
15. Choi, H.J., Ashok Kumar, N., and Baek J.-B. (2015) Graphene supported non-precious metal-macrocycle catalysts for oxygen reduction reaction in fuel cells. Nanoscale. *7*, 6991-6998.
16. Liu M., Zhang, R., and Chen, W. (2014). Graphene-Supported Nanoelectrocatalysts for Fuel Cells: Synthesis, Properties, and Applications. Chem. Rev. *114*, 5117-5160.
17. Bae, S., Kim, H., Lee, Y., Xu, X., Park, J.-S., Zheng, Y., Balakrishnan, J., Lei, T., Ri Kim, H., Song, Y. I., et al, (2010). Roll-to-roll production of 30-inch graphene films for transparent electrodes. Nat. Nanotechnol., *5*, 574-578.
18. Lin, Y.-M., Dimitrakopoulos, C., Jenkins, K. A., Farmer, D. B., Chiu, H.-Y., Grill, A., and Avouris, P. (2010). 100-GHz Transistors from Wafer-Scale Epitaxial Graphene. Science. *327*, 662-662.
19. Dirian, K., Herranz, M. A., Katsukis, G., Malig, J., Rodríguez-Pérez, L., Romero-Nieto, C., Strauss, V., Martín, N., and Guldi, D. M. (2013). Low dimensional nanocarbons – chemistry and energy/electron transfer reactions. Chem. Sci., *4*, 4335-4353.
20. Mateos-Gil, J., Rodriguez-Perez, L., Moreno Oliva, M., Katsukis, G., Romero-Nieto, C., Herranz, M. A., Guldi, D. M., and Martin, N. (2015). Electroactive carbon nanoforms: a comparative study via sequential arylation and click chemistry reactions. Nanoscale. *7*, 1193-1200.
21. Hof, F., Schäfer, R. A., Weiss, C., Hauke, F., and Hirsch, A., (2014). Novel λ^3-Iodane-Based Functionalization of Synthetic Carbon Allotropes (SCAs)—Common Concepts and Quantification of the Degree of Addition. Chem. Eur. J. *20*, 16644-16651.
22. Subrahmanyam, K. S., Ghosh, A., Gomathi, A., Govindaraj, A., and Rao, C. N. R. (2009). Covalent and Noncovalent Functionalization and Solubilization of Graphene. Nanosci. Nanotechnol. Lett. *1*, 28-31.
23. Su, Q., Pang, S., Alijani, V., Li, C., Feng, X., and Müllen, K. (2009). Composites of Graphene with Large Aromatic Molecules. Adv. Mater. *21*, 3191-3195.
24. Englert, J. M., Röhrl, J., Schmidt, C. D., Graupner, R., Hundhausen, M., Hauke, F., and Hirsch, A. (2009). Soluble Graphene: Generation of Aqueous Graphene Solutions Aided by a Perylenebisimide-Based Bolaamphiphile. Adv. Mater, *21*, 4265-4269.
25. Xu, Y., Zhao, L., Bai, H., Hong, W., Li, C., and Shi, G. (2009). Chemically Converted Graphene Induced Molecular Flattening of 5,10,15,20-Tetrakis(1-methyl-4-pyridinio)porphyrin and Its Application for Optical Detection of Cadmium(II) Ions. J. Am. Chem. Soc. *131*, 13490-13497.
26. Geng, J., Kong, B.-S., Yang, S. B., and Jung, H.-T. (2010). Preparation of graphene relying on porphyrin exfoliation of graphite. Chem. Commun. *46*, 5091-5093.
27. An, X., Simmons, T., Shah, R., Wolfe, C., Lewis, K. M., Washington, M., Nayak, S. K., Talapatra, S., and Kar, S. (2010). Stable Aqueous Dispersions of Noncovalently Functionalized Graphene from Graphite and their Multifunctional High-Performance Applications. Nano Lett. *10*, 4295-4301.
28. Sampath, S., Basuray, A. N., Hartlieb, K. J., Aytun, T., Stupp, S. I., and Stoddart, J. F. (2013). Direct Exfoliation of Graphite to Graphene in Aqueous Media with Diazaperopyrenium Dications, Adv. Mater. *25*, 2740-2745.
29. Zhang, F., Chen, X., Boulos, R. A., Md Yasin, F., Lu, H., Raston, C., and Zhang, H. (2013). Pyrene-conjugated hyaluronan facilitated exfoliation and stabilisation of low dimensional nanomaterials in water. Chem. Commun. *49*, 4845-4847.
30. Kozhemyakina, N. V., Englert, J. M., Yang, G., Spiecker, E., Schmidt, C. D., Hauke, F., and Hirsch, A. (2010). Non-Covalent Chemistry of Graphene: Electronic Communication with Dendronized Perylene Bisimides. Adv. Mater. *22*, 5483-5487.
31. Liu, Z., Liu, Q., Huang, Y., Ma, Y., Yin, S., Zhang, X. Sun, W., and Chen, Y. (2008). Organic Photovoltaic Devices Based on a Novel Acceptor Material: Graphene. Adv. Mater. *20*, 3924-3930.
32. Castelain, M., Salavagione, H. J., Gomez, R., and Segura, J. L. (2011). Supramolecular assembly of graphene with functionalized poly(fluorene-alt-phenylene): the role of the anthraquinone pendant groups. Chem. Commun. *47*, 7677-7679.
33. Malig, J., Jux, N., and Guldi, D. M. (2013) Toward Multifunctional Wet Chemically Functionalized Graphene—Integration of Oligomeric, Molecular, and Particulate Building Blocks that Reveal Photoactivity and Redox Activity. Acc. Chem. Res. *46*, 53-64.
34. Fukuzumi, S., and Kojima, T. (2008). Photofunctional nanomaterials composed of multiporphyrins and carbon-based π-electron acceptors. J. Mater. Chem. *18*, 1427-1439.
35. Herranz, M. Á., Ehli, C., Campidelli, S., Gutiérrez, M., Hug, G. L., Ohkubo, K., Fukuzumi, S., Prato, M., Martín, N., and Guldi, D. M. (2008). Spectroscopic Characterization of Photolytically Generated Radical Ion Pairs in Single-Wall Carbon Nanotubes Bearing Surface-Immobilized Tetrathiafulvalenes. J. Am. Chem. Soc. *130*, 66-73.
36. Bikram K. C, C., Das, S. K., Ohkubo, K., Fukuzumi, S., and D'Souza, F. (2012). Ultrafast charge separation in supramolecular tetrapyrrole–graphene hybrids. Chem. Commun. *48*, 11859-11861.
37. Roth, A., Ragoussi, M.-E., Wibmer, L., Katsukis, G., Torre, G. d. l., Torres, T., and Guldi, D. M. (2014). Electron-accepting phthalocyanine–pyrene conjugates: towards liquid phase exfoliation of graphite and photoactive nanohybrid formation with graphene. Chem. Sci. *5*, 3432-3438.
38. Villegas, C., Krokos, E., Bouit, P.-A., Delgado, J. L., Guldi, D. M., and Martin, N., (2011). Efficient light harvesting anionic heptamethine cyanine–[60] and [70]fullerene hybrids, Energy Environ. Sci. *4*, 679-684.
39. Bouit, P.-A., Spänig, F., Kuzmanich, G., Krokos, E., Oelsner, C., Garcia-Garibay, M. A., Delgado, J. L., Martín, N., and Guldi, D. M. (2010) Efficient Utilization of Higher-Lying Excited States to Trigger Charge-Transfer Events. Chem. Eur. J. *16*, 9638-9645.
40. Nieto, C. R., Guilleme, J., Villegas, C., Delgado, J. L., Gonzalez-Rodriguez, D., Martin, N., Torres, T., and Guldi, D. M. (2011).Subphthalocyanine-polymethine cyanine conjugate: an all organic panchromatic light harvester that reveals charge transfer. J. Mater. Chem. *21*, 15914-15918.
41. In the following, the term graphene is also used for few layer graphene for simplification.
42. Rodríguez-Pérez, L., García, R., Herranz, M. Á., and Martín, N. (2014). Modified SWCNTs with Amphoteric Redox and Solubilizing Properties. Chem. Eur. J. *20*, 7278-7286.
43. Tseng, T.-C., Urban, C., Wang, Y., Otero, R., Tait, S. L., Alcamí, M. Écija, D., Trelka, M., Gallego, J. M., Lin, et al., (2010).Charge-transfer-induced structural rearrangements at both sides of organic/metal interfaces. Nat. Chem. *2*, 374-379.
44. Maciel, I. O., Anderson, N., Pimenta, M. A., Hartschuh, A., Qian, H., Terrones, M., Terrones, H., Campos-Delgado, J., Rao, A. M., Novotny, L., et al. (2008). Electron and phonon renormalization near charged defects in carbon nanotubes, Nat. Mater. *7*, 878-883.
45. Voggu, R., Rout, C. S., Franklin, A. D., Fisher, T. S., and Rao, C. N. R. (2008) Extraordinary Sensitivity of the Electronic Structure and Properties of Single-Walled Carbon Nanotubes to Molecular Charge-Transfer. J. Phys. Chem. C, *112*, 13053-13056.
46. Dong, X., Fu, D., Fang, W., Shi, Y., Chen, P., and Li, L.-J. (2009). Doping Single-Layer Graphene with Aromatic Molecules. Small. *5*, 1422-1426.